A Structural Variation for MurB: X-ray Crystal Structure of *Staphylococcus aureus* UDP-*N*-Acetylenolpyruvylglucosamine Reductase (MurB)‡

Timothy E. Benson,*,⊥ Melissa S. Harris,⊥ Gil H. Choi,§ Joyce I. Cialdella,⊥ John T. Herberg,⊥ Joseph P. Martin, Jr.,⊥ and Eric T. Baldwin⊥

Structural, Analytical, and Medicinal Chemistry, Biology, and Protein Science, Pharmacia Corporation, 301 Henrietta Street, Kalamazoo, Michigan 49007, Molecular Biology, Human Genome Sciences, Inc., 9410 West Key Avenue, Rockville, Maryland 20850

Received September 14, 2000; Revised Manuscript Received January 2, 2001

ABSTRACT: The X-ray crystal structure of the substrate free form of *Staphylococcus aureus* UDP-*N*-acetylenolpyruvylglucosamine reductase (MurB) has been solved to 2.3 Å resolution with an R-factor of 20.3% and a free R-factor of 22.3%. While the overall fold of the *S. aureus* enzyme is similar to that of the homologous *Escherichia coli* MurB X-ray crystal structure, notable distinctions between the *S. aureus* and *E. coli* MurB protein structures occur in residues involved in substrate binding. Analysis of available MurB sequences from other bacteria suggest that the *S. aureus* MurB structure is representative of a distinct structural class of UDP-*N*-acetylenolpyruvylglucosamine reductases including *Bacillus subtilis* and *Helicobacter pylori* that are characterized by a modified mechanism for substrate binding.

Reports of an increase in antibiotic resistant bacteria have stimulated efforts to find new classes of therapeutic agents that will prevent society from entering a "post-antibiotic age" (*1*). Historically, three important cellular functions have been the major targets of antibiotics: cell wall biosynthesis, DNA replication, and protein translation. The biosynthesis of the bacterial cell wall, in particular the peptidoglycan polymer, is a particularly attractive target since this flexible structure provides protection for the cell against osmotic lysis (*2*). To date, most of the therapeutic agents discovered that target cell wall biosynthesis inhibit the later stages of peptidoglycan biosynthesis at the point where interstrand cross linking occurs between the peptide chains. Recent efforts have been directed toward purifying and characterizing all the enzymes in the peptidoglycan biosynthetic pathway with the hope that novel enzyme inhibitors might be found for these essential targets.

Bacterial peptidoglycan is a polymer that includes a repeating disaccharide subunit of *N*-acetylglucosamine and *N*-acetylmuramic acid and an extended four to five residue amino acid chain. The first step toward creating this peptidoglycan polymer involves the formation of UDP-*N*-acetylmuramic acid from UDP-*N*-acetylglucosamine by the enzymes MurA and UDP-*N*-acetylenolpyruvylglucosamine reductase (MurB).[1] MurA catalyzes the first stage of this transformation by transferring the enolpyruvate moiety of phosphoenolpyruvate to the 3′ hydroxyl of UDP-*N*-acetylglucosamine with the release of inorganic phosphate (*3*−*4*). The resulting product, enolpyruvyl-UDP-*N*-acetylglucosamine (EP-UDPGlcNAc), undergoes a reduction catalyzed by the MurB enzyme (*5*) by utilizing one equivalent of NADPH and a solvent-derived proton (*6*). This two-electron reduction creates the lactyl ether of UDP-*N*-acetylmuramic acid upon which a five-residue peptide chain is built. Construction of this pentapeptide is catalyzed in a nonribosomal fashion by the enzymes MurC (*7*−*8*), MurD (*9*), MurE (*10*−*11*), and MurF (*12*) (Figure 1) in both Gram-negative bacteria such as *Escherichia coli* and Gram positive bacteria such as *Staphylococcus aureus*. The resulting UDP-*N*-acetylmuramyl pentapeptide is subsequently attached to an undecaprenyl lipid moiety by MraY (*13*) and joined to another sugar, UDP-*N*-acetylglucosamine, by MurG (*14*−*15*). In *Staphylococci*, the next steps of peptidoglycan biosynthesis involve another family of enzymes, FemX, FemA, and FemB, which create a pentaglycine strand in a stepwise fashion on the amino terminus of the lysine side chain (*16*−*18*). This extended Lys-Gly_5 chain serves as the interstrand bridge between nearby peptide strands. Cross-linking between strands can then occur between the lysine-pentapeptide bridge and the carbonyl of the fourth residue (D-Ala) with release of the terminal D-Ala in a transpeptidation step catalyzed by penicillin binding proteins (*19*−*21*).

While several laboratories have characterized many of the Mur enzymes for *E. coli* including the structures of MurA (*22*), MurB (*23*), MurD (*24*), MurF (*25*), and MurG (*26*), little biochemistry or structural biology has been carried out on these enzymes from a clinically relevant Gram-positive

‡ Atomic coordinates have been deposited in the Protein Data Bank (http://www.rcsb.org) (PDB ID code 1HSK).

* To whom correspondence should be addressed. Phone: (616) 833-9769. Fax: (616) 833-1822. E-mail: timothy.e.benson@pharmacia.com.

⊥ Pharmacia Corporation.

§Human Genome Sciences, Inc.

[1] Abbreviations: MurB, UDP-*N*-acetylenolpyruvylglucosamine reductase; UDPGlcNAc, uridine diphospho-*N*-acetylglucosamine; EP-UDPGlcNAc, uridine diphospho-*N*-acetylglucosamine enolpyruvate; UDPMurNAc, uridine diphospho-*N*-acetylmuramic acid; NADPH, reduced β-nicotinamide adenine dinucleotide phosphate; IPTG, isopropylthio-β-D-galactoside; DTT, dithiothreitol; FAD, flavin adenine dinucleotide; DMSO, dimethyl sulfoxide; MAD, multiple anomalous dispersion.

10.1021/bi002162d CCC: $20.00
Published on Web 02/01/2001

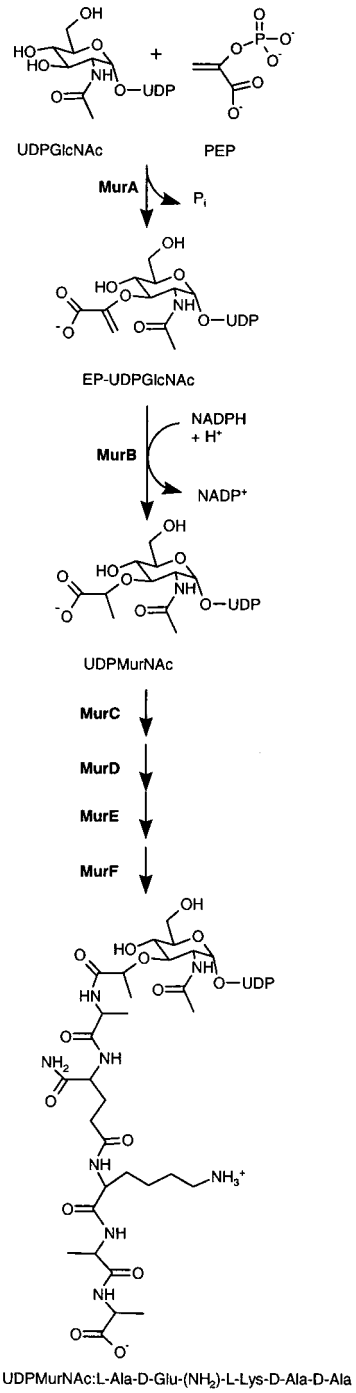

FIGURE 1: Pathway for the biosynthesis of the UDP-*N*-acetylmuramyl pentapeptide showing the first two steps catalyzed by the enzymes MurA and MurB. The UDPMurNAc sugar produced by MurB serves as the point of attachment for the pentapeptide chain built by the related enzymes MurC, MurD, MurE, and MurF.

organism. Interest in the molecular mechanisms of peptidoglycan biosynthesis in Gram-positive organisms has increased in recent years as methicillin-resistant *S. aureus* strains have surfaced that have acquired resistance to the antibiotic vancomycin (*27*). We have chosen to focus our drug discovery efforts on *S. aureus* in an attempt to identify new Gram-positive specific antibacterial agents. Recent access to the entire genome of *S. aureus* has facilitated this process by providing the necessary sequences for the relevant genes of interest. This report describes the first X-ray crystal structure of MurB from a clinically relevant Gram-positive organism and compares it to the previously reported *E. coli* MurB structure.

MATERIALS AND METHODS

Expression of MurB and Incorporation of Selenomethionine. S. aureus MurB (Genbank accession numberAF300988) was expressed using UC 15169, *E. coli* construct K12S (F′ *lacI*^{q}) (pQE-10 murB). MurB cloned into pQE-10 (Qiagen) was obtained from Human Genome Sciences. For expression, the plasmid was transformed into the *E. coli* K12S F′ cell line which has an ampicillin resistance marker. Stock supplies of the culture were maintained at −80 °C in Luria Broth containing ampicillin at 100 μg/mL with 10% glycerol added as a cryopreservative agent.

Seed fermentations were prepared in 100 mL volumes of M9 medium contained in 500-mL wide mouth fermentation flasks. The formulation of basal M9 utilized for these studies was Na_2HPO_4, 6 g; KH_2PO_4, 3 g; NH_4Cl, 1.0 g; and NaCl, 0.5 g per liter of deionized water. The pH was adjusted to 7.4 with concentrated KOH. The medium was sterilized by autoclaving for 30 min. Prior to inoculation, the following filter-sterilized solutions were added per liter of basal medium: 1 M $MgSO_4$, 1.0 mL; 1 M $CaCl_2$, 0.3 mL; trace metal salts solution, 0.3 mL; and 20% glucose, 20 mL. The trace metal salts solution contained per liter of deionized water: $MgCl_2 \cdot 6H_2O$, 39.44 g; $MnSO_4 \cdot H_2O$, 5.58 g; $FeSO_4 \cdot 7H_2O$, 1.11 g; $Na_2MoO_4 \cdot 2H_2O$, 0.48 g; $CaCl_2$, 0.33 g; NaCl, 0.12 g; and ascorbic acid, 1.0 g. Filter-sterilized ampicillin was added to the medium at a final concentration of 100 μg/mL. A 0.1 mL aliquot of the stock culture was inoculated into the medium and allowed to grow at 37 °C for 18−20 h with a shaking rate of 200 rpm. The mature seed culture was harvested by centrifugation and then resuspended in an equal volume of M9 medium. The resuspended seed was used to inoculate expression fermentations at a ratio of seed culture volume to culture medium volume of 0.03:1.

For expression of selenomethionine MurB, M9 media was again utilized in 100 mL volumes containing 100 μg/mL of ampicillin. Multiple flasks were employed to achieve the desired production volume. Since UC 15169 is not a methionine auxotroph, incorporation of selenomethionine was accomplished through down-regulation of methionine biosynthesis just prior to induction of MurB expression with IPTG, isopropyl thio-β-D-galactosidase (*23*, *28*). The culture was grown at 37 °C with a shaking rate of 200 rpm until an A_{600} of ∼0.6. At this point, the following filter-sterilized amino acids were added. L-Lysine, L-threonine, and L-phenylalanine were added to final concentrations of 100 μg/mL. L-Leucine, L-isoleucine, and L-valine were added to final concentrations of 50 μg/mL. Filter-sterilized L-selenomethionine was added simultaneously to a final concentration of 50 μg/mL. After 15−20 min, protein expression was induced by the addition of filter-sterilized IPTG to a final concentration of 1 mM. Growth of the culture was continued at 200 rpm for an additional 4 h until an A_{600} of ∼2.0. This coincided with maximum growth and maximum expression of MurB. Cells were then harvested by centrifugation and frozen at −80 °C. Under these conditions, the average yield of cell paste was 4−4.5 g/L. Selenomethionyl MurB comprised roughly 2−5% of the total cell protein with >75% expressed in the soluble form.

Purification of Selenomethionine MurB. All operations were performed at 4 °C and 2-mercaptoethanol and DTT were added to buffers immediately before use. Three hundred milliliters of equilibration buffer (50 mM Tris, pH 7.8, 500 mM NaCl, 10% glycerol, 25 mM imidazole, and 5 mM 2-mercaptoethanol) containing 0.2 mg/mL DNase I (Boehringer Mannheim #104159) was added to 26 g of cell paste obtained from 6 L of fermentation broth and was resuspended by using a Tekmar Tissumizer set on a power setting of 60. The suspension was homogenized by passing it twice through a Rannie homogenizer at 10 000 PSI. The homogenate was centrifuged at 39200*g* for 60 min in a JA20 rotor in a Beckman J2-21 centrifuge. The supernatant was filtered by using a Nalgene 0.2 μm CN filter unit and applied to a Qiagen NTA Superflow column charged with nickel (column volume of 7.9 mL). The column was then washed with 4 column volumes of equilibration buffer and 22 column volumes of wash buffer (50 mM Tris, pH 7.8, 500 mM NaCl, 10% glycerol, 50 mM imidazole, and 5 mM 2-mercaptoethanol) at a flow rate of 108 mL/h and eluted with 2.5 column volumes of elution buffer (50 mM Tris, pH 7.8, 500 mM NaCl, 10% glycerol, 300 mM imidazole, and 5 mM 2-mercaptoethanol) at a flow rate of 60 mL/h. DTT was added to the eluted material to a final concentration of 10 mM and the treated material was dialyzed for 22 h against two changes of nitrogen sparged dialysis buffer (50 mM Tris, pH 7.8, 500 mM NaCl, 10% glycerol, and 10 mM DTT). After dialysis, the sample was sterile filtered, fractionated, and stored at −80 °C.

The protein concentration was 2.42 mg/mL as determined by amino acid analysis. The prepared MurB protein had the correct N-terminal sequence for the first 20 residues. The mass as measured by electrospray mass spectrometry indicated the full incorporation of the five selenomethionines into the protein. Amino acid analysis gave a correlation coefficient of 0.99 between the recovered and theoretical amino acid composition, indicative not only of high purity but also of the correct amino acid composition in the protein.

Protein Crystallization. Protein samples were buffer exchanged into 20 mM Hepes, pH 7.5, 5 mM 2-mercaptoethanol and concentrated to 20 mg/mL using an Ultrafree 0.5 centrigual filters with a Biomax 10K membrane (Millipore, Bedford, MA). Selenomethionine MurB crystals were grown in 3μL + 3μL sitting drops in 9.75% PEG 8000, 0.1 M cacodylic acid, pH 6.5, 0.55 M ammonium sulfate, 20% DMSO, 5 mM 2-mercaptoethanol with 1 mM EP-UDPGlcNAc substrate. These conditions were originally identified by screening for crystallization conditions with the methionine incorporated *S. aureus* MurB. The hexagonal shaped crystals grew over a period of two to three weeks. The mother liquor served as the cryoprotectant for freezing during data collection at 100 K in liquid nitrogen.

Data Collection and Structure Determination. Access to synchrotron radiation at the Advance Photon Source at Argonne National Labs (IMCA-CAT, Beamline 17-ID) afforded the opportunity to solve the *S. aureus* MurB structure by multiple anomalous dispersion (MAD) phasing. EXAFS analysis revealed a sharp selenium K edge for the selenomethionine MurB (data not shown). A three wavelength experiment was carried out with a low energy wavelength (12 000 eV, 1.0332 Å), a wavelength corresponding to the inflection point of the absorption edge (12 659.4 eV, 0.97939 Å), and a wavelength collected at the peak of the absorption edge (12 660.8 eV, 0.97928 Å). All diffraction data were collected on a 2k by 2k Brüker CCD detector.

Table 1: Data Collection and Phasing Statistics

	λ 1.0332 Å (12 000 eV)	λ 0.97939 Å (12 659.4 eV)	λ 0.97928 Å (12 660.8 eV)
resolution (Å)	2.3	2.3	2.3
no. observations	252 156	267 578	268 391
no. unique refl.	39 984	40 336	40 394
% completeness	94.4	95.2	95.3
R_{sym} (%)	7.5	9.5	9.4
R_{cullis} acentrics		0.77	0.83
R_{cullis} anomalous	0.99	0.84	0.84
phasing power			
centrics		0.87	0.69
acentrics		0.77	0.83
mean figure of merit (to 2.3 Å resolution)			
before solvent flattening		0.464	
after solvent flattening		0.605	

Data sets at each wavelength were processed separately with the program SAINT (Siemens Analytical X-ray Systems, Madison, WI) while keeping the anomalous pairs separate (Table 1). The inflection point and peak data sets were scaled to the remote energy data set using SCALEIT in CCP4 (*29*) by treating the remote wavelength as native. Anomalous and dispersive difference Patterson maps showed strong signals for four of the five selenium atoms suggesting the N-terminal methionine was disordered. Locations of the selenium sites were determined using the automated Patterson solution routine in SHELX (*30*). The location of each selenium site was confirmed by the ability of individual sites to generate phases that could identify the other sites in cross difference Fourier calculations. All heavy atom parameter refinement and phasing calculations were carried out with MLPHARE (*29*, *31*) by treating the remote wavelength as native and the edge and peak wavelengths as derivatives (*32*). The phases were subsequently subjected to solvent flattening using the program DM (*29*, *33*, *34*).

Model building was performed using the program CHAIN (*35*). The *E. coli* MurB model was used as a template for model building to speed the placement of the main chain atoms. All refinement steps were carried out using XPLOR 3.8.5.1 and XPLOR 98.0 (*36*) against the 1.0332 Å (low energy) data set. Several rounds of torsional dynamics (*37*) and simulated annealing (*38*) with rebuilding after each round of refinement were carried out. In the later stages of refinement, a bulk solvent model was included to properly account for inclusion of lower resolution data (*39*). Progress of the refinement was monitored by the free R factor that was calculated for 10% of the reflections that were not included in refinement (*40*). Analysis by PROCHECK showed good main chain geometry and side chain torsion angles (*41*). Figure 4 was made with Molscript 2.1 (*42*) and Raster3D (*43*), and Figures 6 and 10 were made with Molscript 2.1 only.

RESULTS

Structure Solution. Crystals of *S. aureus* MurB in the cubic space group $I2_13$ with cell constants $a = b = c = 178.9$ Å,

```
  1 MRGSHHHHHHTDPINKDIYQALQQLIPNEKIKVDEPLKRYTYTKTGGNAD
                                                  ||  :    ||
  1 ..............................MDHSLKPWNTFGIDHNAQ

 51 FYITPTKNEEVQAVVKYAYQNEIPVTYLGNGSNIIIREGGIRGIVISLLS
      :      ::.     .||      ||   || |||::   |      ::|. :
 19 HIVCAEDEQQLLNAWQYATAEGQPVLILGEGSNVLFLEDYRGTVIINRIK

101 LDHIEVSDDA..IIAGSGAAIIDVSRVARDYALTGLEFACGIPGSIGGAV
      |     ||  :  |.|     . :       : |||     ||| :| .
 69 GIEIHDEPDAWYLHVGAGENWHRLVKYTLQEGMPGLENLALIPGCVGSSP

149 YMNAGAYGGEVKDCIDYALCVN.EQGSLIKLTTKELELDYRNSIIQKEH.
      | |||| |..     |    |    |  ::|| ||     ||.|| . |:
119 IQNIGAYGVELQRVCAYVDSVELATGKQVRLTAKECRFGYRDSIFKHEYQ

197 ..LVVLEAAFTLAP........GK.......MTEIQAKMDDLTERRESKQ
       ..     |                                |   .  .   | .|
169 DRFAIVAVGLRLPKEWQPVLTYGDLTRLDPTTVTPQQVFNAVCHMRTTKL

230 P..LEYPSCGSVFQRP............PG..............HFAGKL
    |       .  || |. |                              || |
219 PDPKVNGNAGSFFKNPVVSAETAKALLSQFPTAPNYPQADGSVKLAAGWL

252 IQDSNLQGHRIGGVEVSTKHAGFMVNVDNGTATDYENLIHYVQKTVKEKF
    |     |.| .|||   |   . |   ::| ||   .  |     | |:|.. | |||
269 IDQCQLKGMQIGGAAVHRQQALVLINEDNAKSEDVVQLAHHVRQKVGEKF

302 GIELNREVRIIGEHPKESLQPSLIS
     : |   ||| ||
319 NVWLEPEVRFIGASGEVSAVETIS.
```

FIGURE 2: Sequence alignment of *S. aureus* and *E. coli* MurB ("|" indicates conserved residues, "." and ":" indicate increasingly similar residues, "..." indicates deletions). Sequence alignment performed using the program GAP (GCG Version 9, Genetics Computational Group, Madison, WI). Modifications to the alignment were made in and near insertion or deletion points to account for similarities and differences based on a comparison of the *S. aureus* and *E. coli* MurB X-ray crystal structures. Residues corresponding to the FAD binding region (domains 1 and 2) are highlighted in blue and those corresponding to the substrate binding region (domain 3) are highlighted in green. Structural features that are present in the *E. coli* but not the *S. aureus* protein are shown in red and were omitted from superpositions. In regions where there are significant deletions in the *S. aureus* protein as compared to the *E. coli* protein, no significance should be given to the placement of the connecting residues in the *S. aureus* sequence. Protein sequence not observed due to disordered electron density for the N and C termini of *S. aureus* MurB are underlined.

$\alpha = \beta = \gamma = 90°$ diffracted to 2.3 Å resolution. Initial attempts with molecular replacement using the *E. coli* MurB coordinates (*23*) were unsuccessful despite the near 50% similarity with the *S. aureus* sequence (Figure 2). Therefore, an independent set of phases was derived using multiple anomalous dispersion (MAD) with selenomethionine incorporated protein (*44*). *S. aureus* selenomethionine MurB was prepared by inhibiting endogenous methionine biosynthesis while supplementing the expressing cells with selenomethionine (*23*, *28*). Methionine biosynthesis downregulation eliminates the need for transferring the protein expression vector into a *met*$^-$ strain. This technique reduces the time and effort required for producing selenomethionine incorporated protein and results in near quantitative incorporation of selenomethionine into the overexpressed protein. Anomalous and dispersive difference Pattersons revealed the presence of four selenium sites. Solvent-flattened multiple anomalous dispersion phases to 2.3 Å revealed an exceptionally clear electron density map with no significant breaks in the main chain. A portion of the electron density map is shown in Figure 3. The structure was refined to 2.3 Å resolution with an R-factor of 20.3% and a free R-factor of 22.3%. Further details of the structure determination and refinement are described in Tables 1 and 2 and Material and Methods.

Overview of the Structure. S. aureus MurB is composed of three domains (Figures 4 and 5). Domains 1 and 2 are

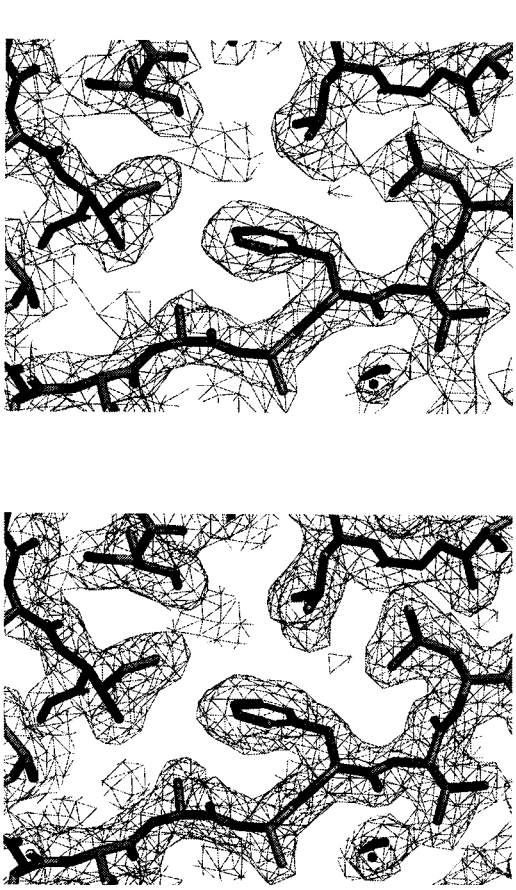

FIGURE 3: Experimental and final electron density maps show the high quality of the experimental MAD phased map. (a) Solvent flattened MAD electron density map at 2.3 Å resolution around residues 202−206 with the final model. (b) Final $2F_o-F_c$ electron density map at 2.3 Å around residues 202−206 with the final model.

Table 2: Refinement Statistics

	R-factor	free R-factor	no. of reflections
10−2.3 Å $F \geq 2\sigma$	20.3%	22.3%	33 156

	bonds (Å)	angles(°)
r.m.s deviation from ideal geometry	0.008	1.37

	no. of atoms	average B-factor
protein	2345	28.4
waters	213	36.6
FAD	53	23.6
total	2611	29.0

responsible for binding of the flavin adenine dinucleotide cofactor while domain 3 is responsible for substrate binding. The rms deviation for all C_α atoms (236 residues out of the 326 *S. aureus* residues) in common between the *E. coli* and *S. aureus* structures is 2.20 Å (Figure 6, panel a). Superpositions for each of the three domains in *S. aureus* as compared to their respective domains in the *E. coli* enzyme resulted in slightly better superpositions for domains 2 and 3 (Figure 6, panels b−d). Domain 1 (residues 14−98) of *S. aureus* MurB has a rms deviation of 2.20 Å for the C_α atoms as compared to *E. coli* MurB. The second domain of *S. aureus* MurB (residues 101−229) has a rms deviation of 1.80 Å for the C_α atoms of the corresponding residues in *E. coli* MurB. The rms deviation for domain 3 of the *S. aureus* enzyme (residues 230−316) is 1.05 Å for the C_α atoms corresponding

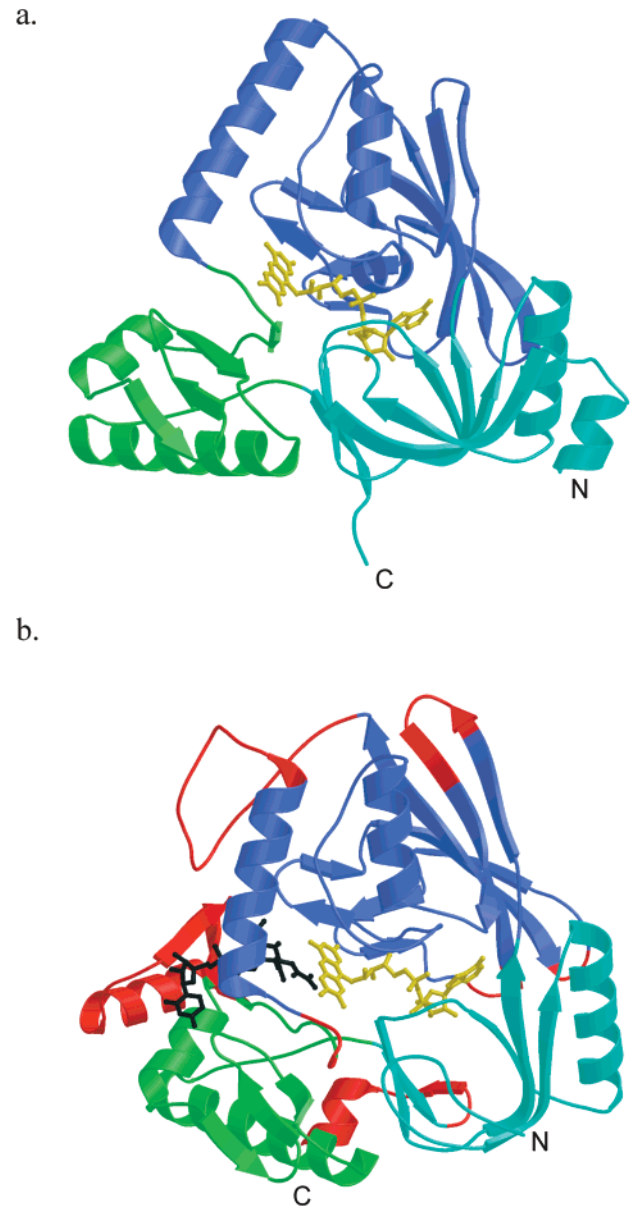

FIGURE 4: Overview of (a) *S. aureus* MurB structure with bound FAD cofactor and (b) *E. coli* MurB structure with bound FAD cofactor and EP-UDPGlcNAc substrate (*23*). Domain 1 is shown in cyan, domain 2 is shown in blue (domains 1 and 2 comprise the flavin binding domain) and domain 3 is shown in green (substrate binding domain). The flavin cofactor is shown in yellow and the EP-UDPGlcNAc substrate is colored black. Portions of the *E. coli* structure that are absent in the *S. aureus* structure are shown in red.

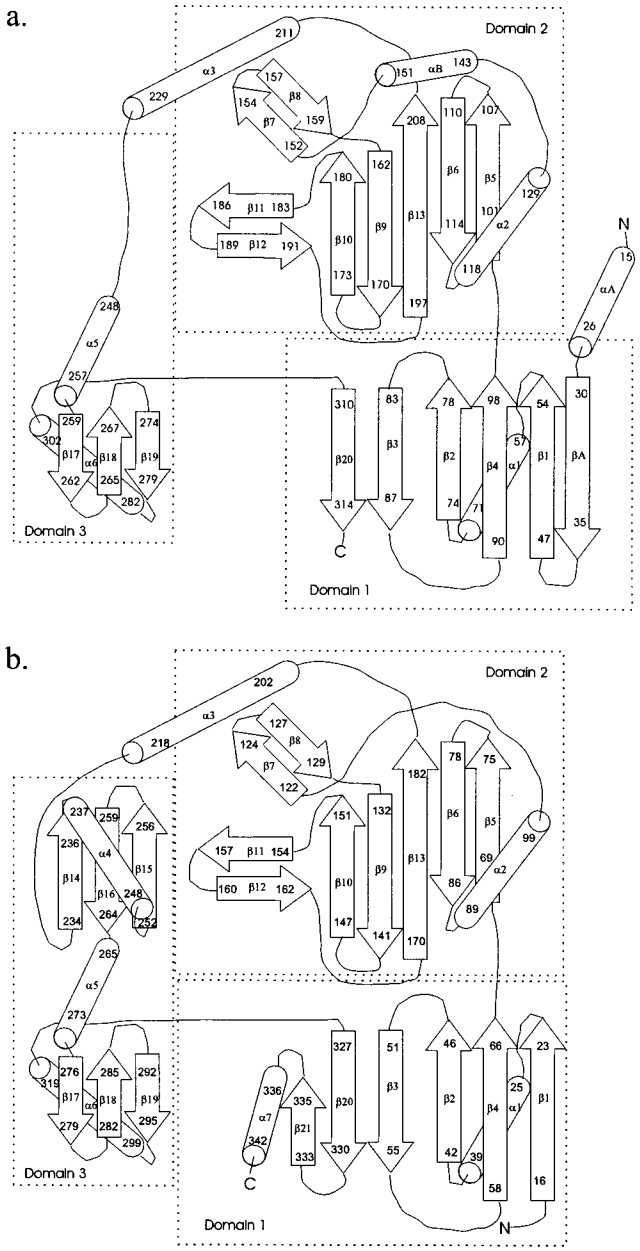

FIGURE 5: Secondary structure diagram for (a) *S. aureus* MurB and (b) *E. coli* MurB. The domain assignments are indicated with a dotted line. Naming of the secondary structure was made to correspond to the previously published *E. coli* MurB structure. Where new elements of secondary structure are present in the *S. aureus* structure, naming begins with "A".

to the portion of this domain present in the *E. coli* structure.

While the overall fold of the *S. aureus* MurB enzyme is similar to that of *E. coli* MurB, several exceptions indicate that the *S. aureus* MurB structure represents a significant structural variation for the UDP-*N*-acetylenolpyruvylglucosamine reductases. The first major difference is the additional 32 amino acids that are present at the N-terminus of *S. aureus* MurB that are not present in the *E. coli* enzyme. While only 18 of these amino acids are observed in the electron density map (the remaining 14 amino acids are disordered), these residues form an additional α helix (αA) and β strand (βA) at the beginning of the peptide chain. (Similar secondary structure elements in *S. aureus* MurB have been given the corresponding names from *E. coli* MurB (*23*) to facilitate the discussion and new elements of secondary structure have been assigned lettered names). The βA strand adds an antiparallel strand to the central parallel β-barrel that forms the base of domain 1. This β-barrel has an extremely hydrophobic core burying the side chains of residues Leu 37, Leu 78, Ile 84, Ile 86, Ile 91, Val 95, and Ile 312.

The second major structural difference in *S. aureus* MurB is the absence of the loop between β13 and α3 (residues 183 to 203 of *E. coli* MurB). To compensate for the loss of this loop, an additional turn of helix is added to α3 to make the connection between β13 and α3 in *S. aureus* MurB. This loop serves an important role in *E. coli* MurB by positioning Tyr 190 to interact directly with the α phosphate of the EP-UDPGlcNAc ligand and to close the active site upon

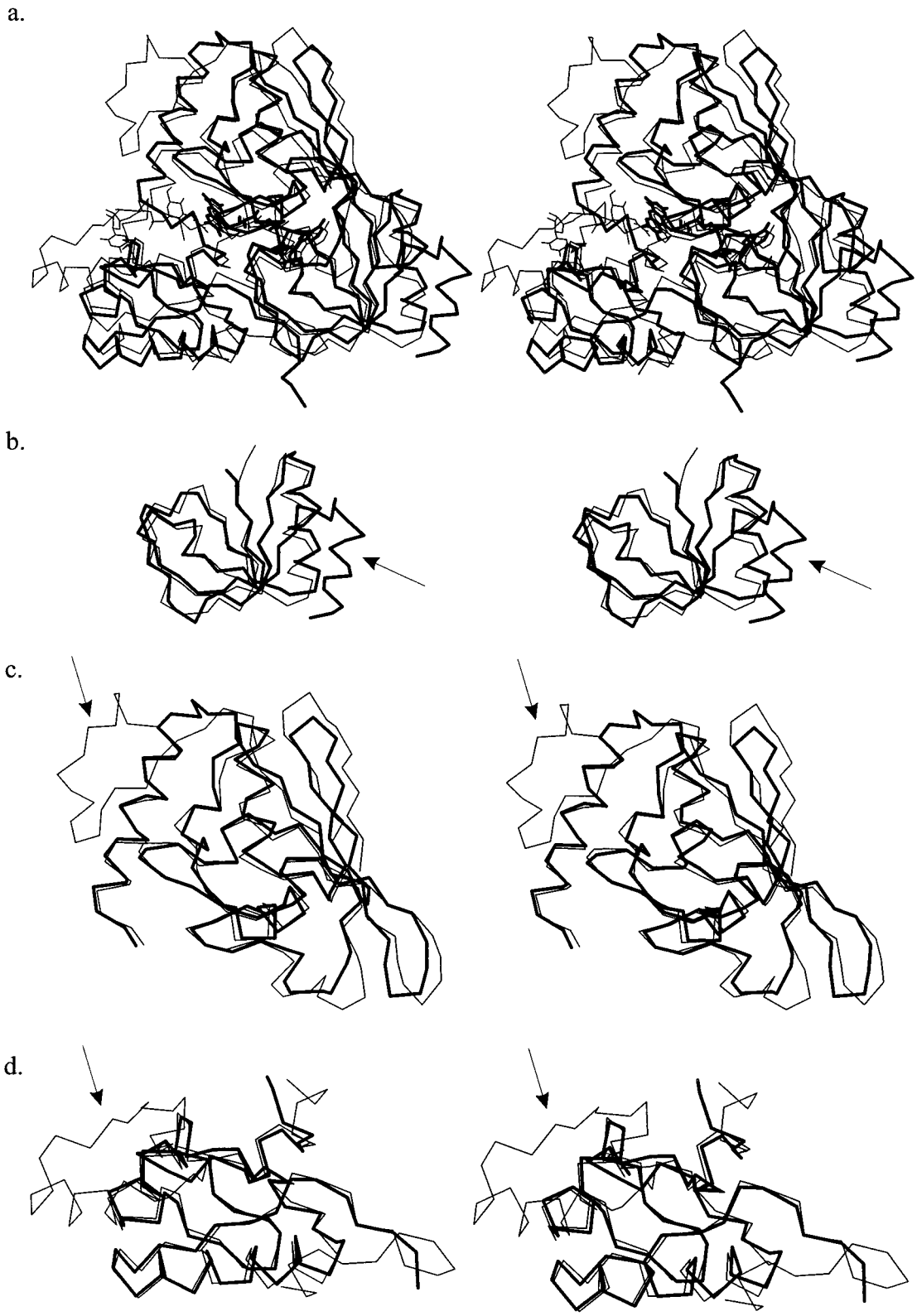

FIGURE 6: Super position of *S. aureus* MurB (thick lines) and *E. coli* MurB (thin lines). Residues used for superpositions of the various domains are described in the text. (a) All C_α atoms in common between the two structures. (b) C_α atoms in domain 1 (lower right of molecule as shown in part a). The arrow points to the additional N-terminal α-helix and *β*-strand present in the *S. aureus* MurB structure. (c) C_α atoms in domain 2 (upper center of molecule as shown in part a). The arrow points to the Tyr 190 loop in the *E. coli* MurB structure that is absent in the *S. aureus* MurB structure. (d) C_α atoms in domain 3 (lower left of molecule as shown in part a). The arrow points to the single split *βαββ* fold in the *E. coli* MurB structure that is absent in the *S. aureus* MurB structure.

substrate binding (*45*). Observations of the *S. aureus* MurB structure do not reveal any direct substitutes for Tyr 190 suggesting that this specific mechanism for substrate binding observed in *E. coli* MurB is not utilized in the *S. aureus* enzyme. In the *E. coli* MurB structure, the α phosphate of the EP-UDPGlcNAc also interacts with the side chain of Lys 217. This residue is conserved in the *S. aureus* MurB structure as residue Lys 228. Therefore, one would expect

that the absence of Tyr 190 would lead to an increased importance for Lys 228 in the formation of a productive enzyme−substrate complex in *S. aureus* MurB. The third major structural difference is the deletion of a portion of the substrate binding domain in the *S. aureus* MurB protein structure. One of the α + β motifs present in the *E. coli* structure, the single split βαββ fold (β14, α4, β15, β16) is absent in the *S. aureus* MurB structure. This portion of the *E. coli* structure provides several van der Waals contacts with the EP-UDPGlcNAc ligand. In the absence of this portion of the substrate binding domain, the ligand binding surface on *S. aureus* MurB is notably more narrow.

Several minor differences in the main chain between the two structures are also observed. First, in the *E. coli* MurB, two residues in β5 and β6 are not found in the *S. aureus* MurB structure resulting in two shorter β-strands for the *S. aureus* enzyme. Second, the hydrogen bonding distances and geometries for residues 143−151 in *S. aureus* MurB are consistent with a secondary structure assignment of an α-helix (αB) for these residues in the core of the protein. This same region in the *E. coli* structure (residues 113−121) shows secondary structure similar to an α-helix with allowed φ and ψ angles, but with poor hydrogen bonding distances and geometries; therefore, this region was not assigned as an α-helix in the original *E. coli* MurB structure (*23*). Third, a single residue deletion in the *S. aureus* structure occurs in the loop between β9 and β10 leading to a shorter connection between these two strands. Finally, the last β-strand (β21) and α-helix (α7) in the *E. coli* MurB structure are not observed in the *S. aureus* MurB structure. The exact secondary structure of these residues is unknown since the last nine residues of the C terminus of *S. aureus* MurB are disordered in the electron density map.

Flavin Cofactor Binding. The conserved protein fold of MurB in the *S. aureus* enzyme is particularly pronounced for the flavin binding portion of the molecule (domains 1 and 2, Figure 6, panels b and c). Not only is the flavin binding fold conserved, but also the conformation of the flavin adenine dinucleotide ligand is nearly identical between the two structures (rms deviation for all of the cofactor atoms comparing the *S. aureus* FAD and the *E. coli* FAD is 0.30 Å). This FAD binding fold in both MurB structures is a member of a new superfamily of flavin adenine dinucleotide binding proteins (*46*). The other members of this FAD binding protein family for which protein structures have been solved include *p*-cresol methylhydroxylase from *Pseudomonas putida* (*47*), vanillyl-alcohol oxidase from *Penicllium simplicissimum* (*48*), and CO dehydrogenase from *Oligotropha carboxidovorans* (*49*).

The protein side chain and main chain interactions with the FAD cofactor found in the *S. aureus* enzyme are mostly similar to those interactions observed in *E. coli* MurB. The N5 and O4 of the isoalloxazine ring of the flavin adenine dinucleotide interact with the guanidinium moiety of Arg 225 in a manner similar to that observed for Arg 214 in the *E. coli* MurB structure (Figure 7). The sequence and positional conservation of this arginine in the structure suggests that it plays a role in the binding of the flavin and stabilization of the reduced cofactor during catalysis. Two other interactions to the isoalloxazine ring (N3 and O2) are maintained by the main chain nitrogen and carbonyl oxygen of Gly 153. Interactions with the ribityl sugar moiety are also similar to those observed in the *E. coli* MurB. The carbonyl oxygen of Pro 141 and the hydroxyl group of Ser 82 make hydrogen bonds to the first hydroxyl group and the carbonyl of Gly 146 interacts with the third hydroxyl moiety. The extensive interactions between the protein and the diphosphoadenine portion of the molecule are also well conserved with the main chain atoms of residues 79−83 that include the Gly−X−Gly motif found in the Rossmann fold (*50*) and provide important stabilizing interactions with the two phosphates. Two serines (Ser 82 and Ser 143) again serve to make specific contacts with the β phosphate moiety but using a geometry different from *E. coli* MurB. The placement of Ser 82 is conserved with respect to its counterpart in *E. coli* MurB (Ser 50), but Ser 143 is three residues away (one turn of α-helix B) from the position corresponding to the *E. coli* MurB Ser 116. While this places the serine hydroxyl on the opposite site of the phosphate (when compared to the *E. coli* MurB), the hydrogen bonding interaction is maintained. Finally, two residues make contacts to the 3′-hydroxyl of the ribityl sugar, Tyr 149 and Arg 310. The corresponding residues in *E. coli* MurB for Tyr 149 is Ile 149 that does not make any hydrogen bonds to the ribityl sugar but does make hydrophobic interactions with this part of the flavin. The substitution of tyrosine in *S. aureus* MurB at this position allows for both hydrogen bonding and hydrophobic contacts.

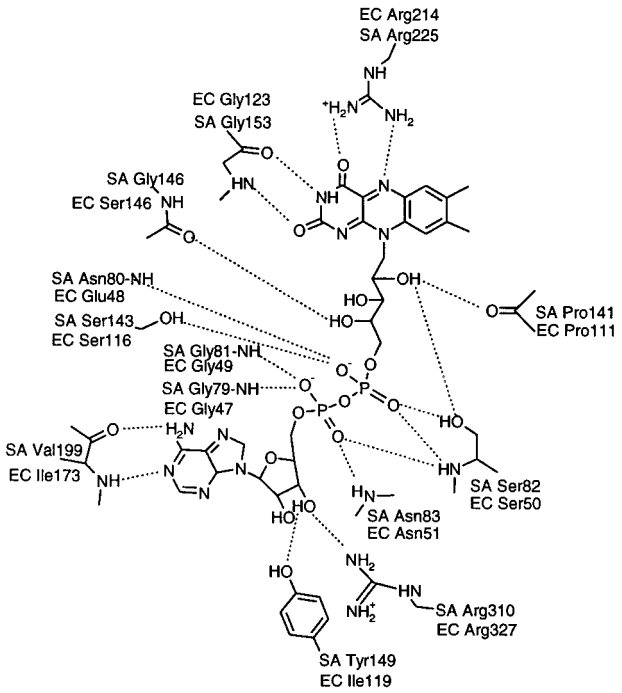

FIGURE 7: Schematic view of side chain and main chain interactions between *S. aureus* MurB and the FAD cofactor. Residues for the *S. aureus* enzyme are indicated adjacent to the amino acid and the corresponding residues for the *E. coli* enzyme are shown in parentheses. Distances that would allow hydrogen bonds with the FAD are shown as dotted lines.

Active Site Arrangement and Implications for Substrate Binding. The electron density map in the active site of *S. aureus* MurB reveals regions of disconnected electron density that did not clearly resemble the EP-UDPGlcNAc substrate despite the presence of the substrate in the crystallization conditions. Therefore, the exact location and interactions between *S. aureus* MurB and the EP-UDPGlcNAc substrate

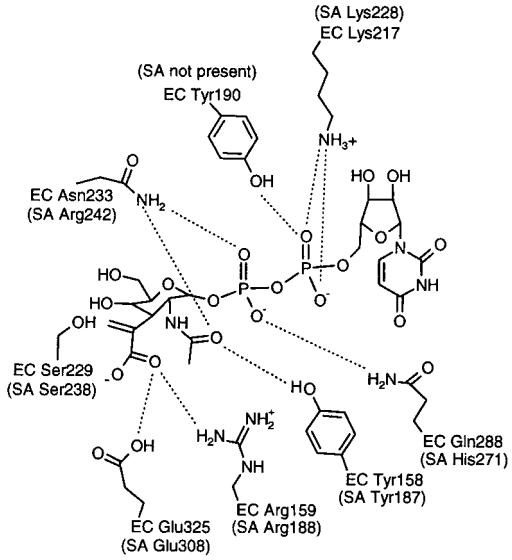

FIGURE 8: Proposed binding interactions of *S. aureus* MurB with the EP-UDPGlcNAc substrate based on the *E. coli* MurB structure. Residues involved in EP-UDPGlcNAc binding in *E. coli* MurB are shown in shown in parentheses.

in the active site cannot be determined at this time. Comparison of the *S. aureus* and *E. coli* structures reveals strict conservation of the active site residues. The three catalytic active site residues in *E. coli*, Arg 159 and Glu 325 that would stabilize the C2 acicarbanionic species and Ser 229 that would provide a proton to quench the intermediate, are strictly conserved in the *S. aureus* active site, Ser 238, Arg 188, and Glu 308 (Figure 8) (*23*). In addition, two residues that were shown to play a role in substrate binding in the *E. coli* enzyme are also strictly conserved in the active site of *S. aureus* MurB (Tyr 187 and Lys 288). Two other residues shown to be important for substrate binding, Asn 233 and Gln 288, are replaced in the *S. aureus* structure by Arg 242 and His 271, respectively. The only critical substrate binding residue that is not found in the *S. aureus* structure is the *E. coli* Tyr 190 that is absent due to the deletion of the loop between β13 and α3 in *S. aureus* protein as previously noted. The absence of this single residue does not appear to compromise the ability of the enzyme to bind substrate since all of the other hydrogen bond interactions observed in the *E. coli* MurB structure would be maintained.

DISCUSSION

A comparison of the two MurB structures reveals that the *S. aureus* MurB possesses the same general fold that was observed in the *E. coli* MurB structure, an $\alpha + \beta$ protein with three domains. Two of these domains create a binding site for the flavin adenine dinucleotide cofactor and the third domain participates in substrate binding. On the basis of the high similarity between the two protein sequences, a related fold was clearly expected. Yet, it is not surprising that differences between the two structures are evident in the substrate binding regions of the enzymes, since the sequence alignment reveals regions of significant deletions.

The most relevant deletions that occur in the *S. aureus* MurB structure involve portions of the enzyme that play an important part in the binding of EP-UDPGlcNAc (*23*) or NADPH (*51*−*52*) in *E. coli* MurB. The loop between β13 and α3 in *E. coli* MurB contains Tyr 190 which undergoes a dramatic motion upon EP-UDPGlcNAc binding. The absence of this loop and its key residue in the *S. aureus* structure suggests that ligand binding in this bacterial species has adapted to compensate for the loss of Tyr 190. The K_m for EP-UDPGlcAc with *S. aureus* MurB is 15 μM, while the K_m for NADPH is 40 μM (S. Swaney, personal communication) which are of the same magnitude as the K_m values for EP-UDPGlcNAc and NADPH with *E. coli* MurB (*6*). These kinetic parameters suggest that the loss of Tyr 190 has little impact on the enzyme's ability to bind either substrate. It is also possible that charged residues from other parts of the molecule could play a role in ligand binding. Interestingly, the other significant deletion also involves a part of the enzyme involved in substrate binding, the single split $\beta\alpha\beta\beta$ fold (β14, α4, β15, and β16 in *E. coli* MurB). This portion of protein structure has a less specific purpose in the mechanism of action of MurB but does serve to provide a surface on which the uridine portion of the EP-UDPGlcNAc substrate rests. Although a three-dimensional NMR structure of the NADPH−*E. coli* MurB complex was never reported, backbone assignments from an *E. coli* MurB−NADPH complex indicate the single split $\beta\alpha\beta\beta$ fold is also important for NADPH binding (*51*−*52*). This observation is consistent with the steady-state kinetic characterization that the *E. coli* MurB catalyzes reduction of the enolpyruvyl group by a ping pong mechanism where both NADPH and EP-UDPGlcNAc utilize the same binding site (*53*).

Although the MurB crystals were grown in the presence of the substrate EP-UDPGlcNAc, no interpretable electron density for the substrate was observed. The failure to obtain a substrate complex could be either the result of weak substrate binding to the enzyme under the conditions necessary for crystallization or the result of crystallization conditions which select for a protein conformation that excludes substrate. Monitoring ligand binding by UV−visible spectroscopy shows the expected red shift of the flavin absorption spectrum associated with EP-UDPGlcNAc as observed with the *E. coli* MurB enzyme (*54*) suggesting that the substrate should be bound to the oxidized form of the *S. aureus* MurB. When the initial crystals did not show the presence of substrate in the active site, higher concentrations of substrate were employed in an attempt to produce a substrate complex. Since the original crystallization buffer was at pH 6.5, crystals were also grown at pH 8.0 within the optimal pH range for the *S. aureus* MurB enzymatic activity. Unfortunately, neither of these changes nor additional crystallization screening efforts identified any crystallization conditions that would support both crystallization of the protein and binding of EP-UDPGlcNAc. Analysis of the packing in the crystal lattice reveals that a symmetry related molecule protrudes into the active site of *S. aureus* MurB in this crystal. Specifically, two strands of the major β-sheet (β5 and β6) are situated at the active site opening where the EP-UDPGlcNAc binding site is located. Superimposing the *E. coli* EP-UDPGlcNAc bound structure on the *S. aureus* MurB structure indicates that these strands from the symmetry related molecule would interfere with the binding of the uridine portion of the substrate. These results strongly suggest that the crystal form which is favored during crystallization selects a protein conformation of *S. aureus* MurB that prevents EP-UDPGlcNAc binding.

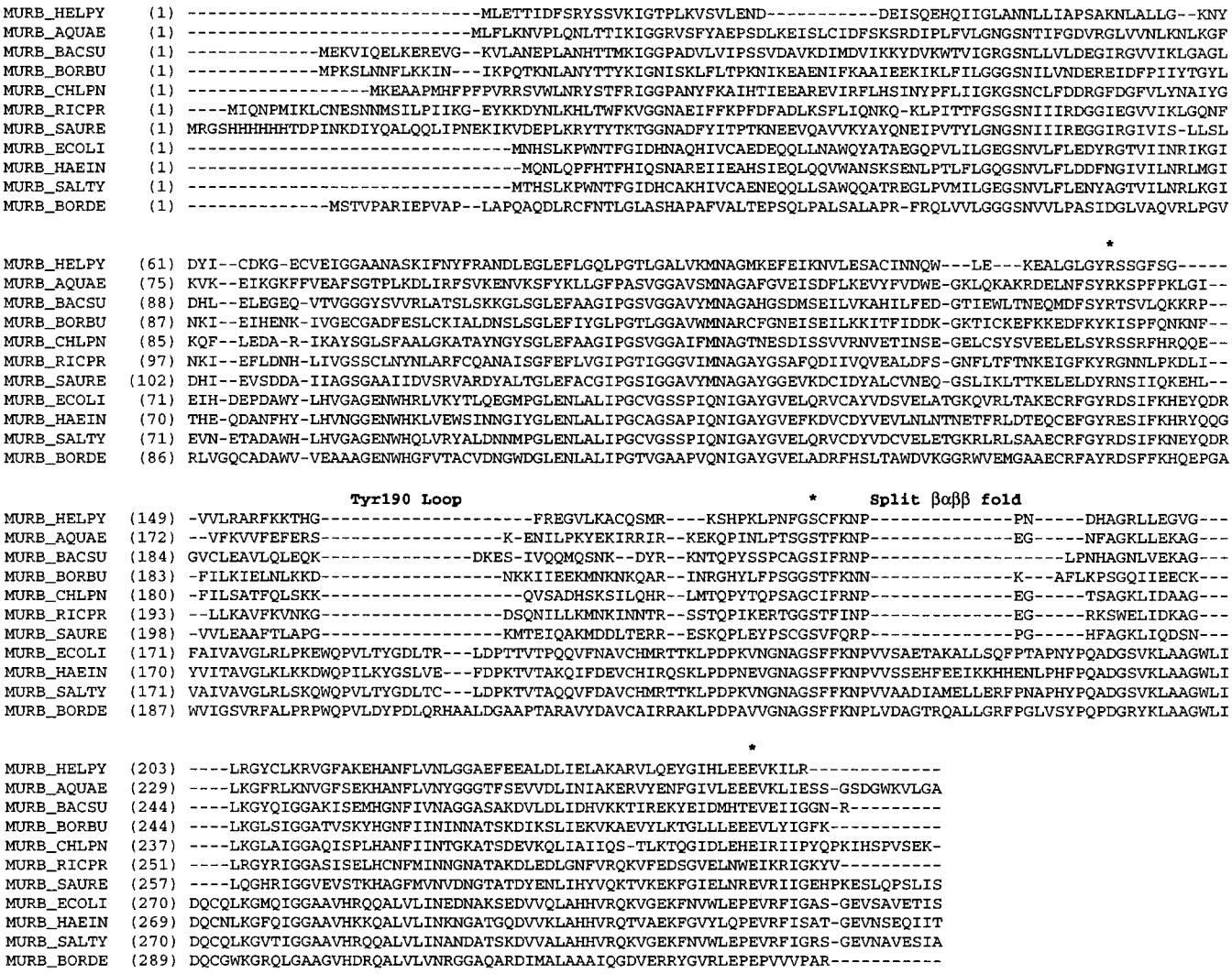

FIGURE 9: Sequence alignment of a representative sample of MurB sequences from Genbank: MURB_HELPY (*Helicobacter pylori*), MURB_AQUAE (*Aquifex aeolicus*), MURB_BACSU (*Bacillus subtilis*), MURB_BORBU (*Borrelia burgdorferi*), MURB_CHLPN (*Chlamydia pneumoniae*), MURB_RICPR (*Rickettsia prowazekii*), MURB_SAURE (*Staphylococcus aureus*), MURB_ECOLI (*Escherichia coli*), MURB_HAEIN (*Haemophilus influenzae*), MURB_SALTY (*Salmonella typhimurium*), MURB_BORDE (*Bordetella pertussis*). Asterisks indicate the proposed active site residues involved in catalysis. Several other MurB sequences were not included in this alignment including *Treponema pallidum* MurB (class II MurB) and *Mycobacterium tuberculosis* MurB (class I MurB) because of additional insertions or deletions in these protein sequences that complicated the multiple sequence alignment.

Fortunately, placement of the EP-UDPGlcNAc substrate can be inferred from the *E. coli* MurB-EP-UDPGlcNAc structure. The active site for MurB is defined by residues that stabilize the intermediate produced when a hydride is transferred from N1 to C3 of the enolpyruvyl group and facilitate the quenching of this intermediate. On the basis of *S. aureus* MurB structure, a mechanism was proposed for stabilization of this acicarbanonic species by charge neutralization and/or by protonation. As in the *E. coli* model, two residues, Arg 188 and Glu 308, exist that could serve this mechanistic purpose. Similarly, Ser 238 corresponds to *E. coli* MurB Ser 229 that is proposed to serve as a general acid catalyst in conjunction with an active site water (*55*). The Ser 238 hydroxyl is 6.3 Å away from N1 of the FAD cofactor in the *S. aureus* MurB structure. Since the corresponding serine hydroxyl is similarly positioned (6.1 Å from N1) in the *E. coli* MurB structure, it appears that *S. aureus* MurB is well-positioned for reduction of the enolpyruvyl group.

An analysis of available MurB sequences in Genbank provides increasing evidence that these three active site residues play critical roles in stabilization and reduction of the C2 acicarbanion intermediate during catalysis. In the sequence alignment shown in Figure 9, the active site glutamate (Glu 308 in *S. aureus* MurB and Glu 325 in *E. coli* MurB) is strictly conserved. The active site arginine (Arg 188 in *S. aureus* MurB and Arg 159 in *E. coli* MurB) is conserved in all species with the exception of *Borrelia burgdorfei* MurB in which a conservative substitution to a lysine is made. The active site serine is equally well conserved across species with the only exception being the MurB sequence from *Chlamydia pneumoniae* where a conservative Cys substitution is present. This conservation of active site residues suggests that mechanistically the UDP-*N*-acetylenolpyruvylglucosamine reductases are equivalent with respect to the reduction of the enolpyruvyl group.

In contrast, these sequence alignments also suggest that there are at least two structural scaffolds for the MurB family. Comparison of the sequences from Genbank reveals that the *S. aureus* MurB is not the only MurB sequence in which the *E. coli* Tyr 190 loop and the single split $\beta\alpha\beta\beta$ fold from the substrate binding domain (β14, α4, β15, and β16 in *E.*

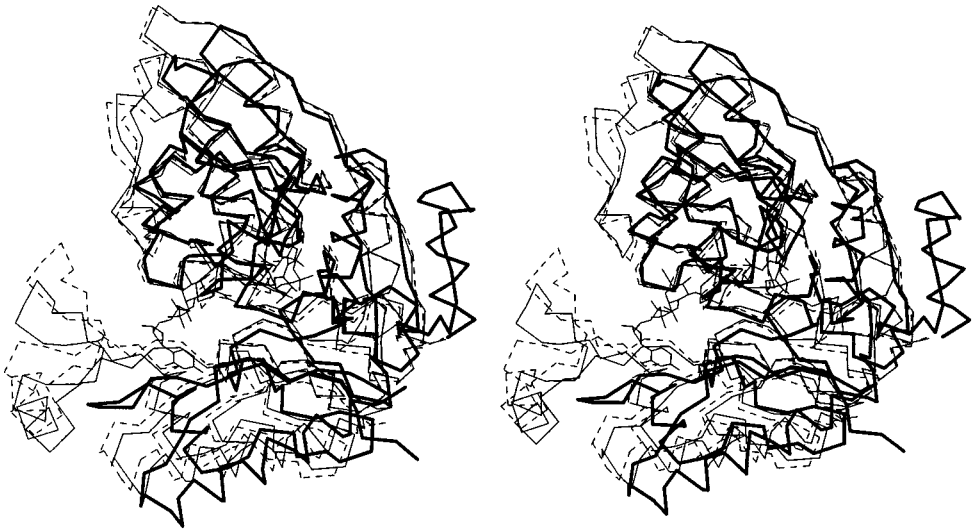

FIGURE 10: C_α backbone traces from three MurB structures (superposition based on the flavin binding domains). The two *E. coli* MurB structures (substrate free *E. coli* MurB shown as dotted lines, EP-UDPGlcNAc bound MurB shown as thin lines) show that the substrate binding domain is actually closer to the flavin binding domain in the absence of substrate than when the substrate is bound. The *S. aureus* MurB structure reveals the greatest displacement of the substrate binding domain from the flavin domain of the three structures.

coli MurB) are absent (Figure 9). This striking similarity among sequences indicates that many of these MurBs from other species would adopt the *S. aureus* MurB type three-dimensional structure as opposed to the *E. coli* MurB type three-dimensional structure. Thus, the trend suggests that at least two distinct classes of MurB protein structures exist, that of the *E. coli* type (type I MurB) and that of the *S. aureus* type (type II MurB), which distinguishes the construction of the substrate binding domain and the manner in which these enzymes bind their substrates.

This classification of two types of MurB consists not only of secondary structural elements that are present or absent but also of how these structural elements define a mode of substrate binding. A comparison of the substrate domain positions between *S. aureus* MurB and the two forms of *E. coli* MurB (substrate free and EP-UDPGlcNAc bound forms) is shown in Figure 10. This superposition reveals that *S. aureus* MurB's substrate binding domain is notably more displaced from domains 1 and 2 in either of the substrate free or the EP-UDPGlcNAc bound forms of *E. coli* MurB. While interactions between crystallographically related molecules hold domain 3 in this open conformation, this displacement reveals the flexibility of the enzyme to achieve an open conformation of the *S. aureus* enzyme with ready access to the ligand binding site. A comparison of the *E. coli* ligand bound and ligand free structure also reveals flexibility of the position of domain 3 with respect to domains 1 and 2. The flexibility of domain 3 in *E. coli* MurB enables ligand binding by an indirect mechanism involving the movement of domain 3 away from the flavin binding domain leading to the disruption of the stacking interaction between Tyr 190 and Tyr 254. This motion allows Tyr 190 to adopt a new rotameric configuration that provides a hydrogen bond to the α phosphate and closes off the active site from the solvent (*45*). In the absence of a residue homologus to Tyr 190 and the loss of the single split $\beta\alpha\beta\beta$ fold (β14, α4, β15, and β16 in *E. coli* MurB), stabilization of the complex must occur by a different mechanism. This process in *S. aureus* MurB most likely involves movement of domain 3 toward the flavin binding domains to hold the substrate in place and close off the active site from solvent during catalysis.

The structure of *S. aureus* MurB demonstrates the subtle yet significant differences that exist among functionally equivalent proteins of various bacterial species. This structure demonstrates the importance of conducting structural and biochemical analysis on the target from the bacterial species of interest to facilitate meaningful drug discovery where the closest possible fit of inhibitor to enzyme is desired. Efforts to identify inhibitors for *S. aureus* UDP-*N*-acetylglucosamine reductase are ongoing.

ACKNOWLEDGMENT

We gratefully acknowledge N-terminal sequencing and amino acid analysis conducted by John G. Hoogerheide and Michele K. Ramsdell, amino acid analysis conducted by June M. Lull, protein mass spectrometry conducted by Diane G. Strother, preparation and purification of EP-UDPGlcNAc conducted by Steven M. Swaney and Robert A. Anstadt, and crystallization support provided by D. Bryan Prince. Use of the Advanced Photon Source was supported by the U.S. Department of Energy, Basic Energy Sciences, Office of Science, under Contract No. W-31-109-Eng-38. Data were collected at beamline 17-ID in the facilities of the Industrial Macromolecular Crystallography Association Collaborative Access Team (IMCA-CAT) at the Advanced Photon Source. These facilities are supported by the companies of the Industrial Macromolecular Crystallography Association through a contract with Illinois Institute of Technology (IIT), executed through the IIT's Center for Synchrotron Radiation Research and Instrumentation. Helpful comments on the manuscript were provided by Robert L. Heinrickson and Barry C. Finzel.

REFERENCES

1. Cohen, M. L. (1992) *Science 257*, 1050−1055.
2. Doyle, R. J., and Marquis, R. E. (1994) *Trends Microbiol. 2*, 57−60.
3. Marquardt, J. L., Siegele, D. A., Kolter, R., and Walsh, C. T. (1992) *J. Bacteriol. 174*, 5748−5752.
4. Brown, E. D., Vivas, E. I., Walsh, C. T., and Kolter, R. (1995) *J. Bacteriol. 177*, 4194−4197.

5. Pucci, M. J., Discotto, L. F., and Dougherty, T. J. (1992) *J. Bacteriol. 174*, 1690−1693.
6. Benson, T. E., Marquardt, J. L., Marquardt, A. C., Etzkorn, F. A., and Walsh, C. T. (1993) *Biochemistry 32*, 2024−2030.
7. Liger, D., Masson, A., Blanot, D., van Heijenoort, J., and Parquet, C. (1995) *Eur. J. Biochem 230*, 80−87.
8. Gubler, M., Appoldt, Y., and Keck, W. (1996) *J. Bacteriol. 178*, 906−910.
9. Dougherty, T. J., Thanassi, J. A., and Pucci, M. J. (1993) *J. Bacteriol. 175*, 111−116.
10. Maruyama, I. N., Yamamoto, A. H., and Hirota, Y. (1988) *J. Bacteriol. 170*, 3786−3788.
11. Michaud, C., Mengin Lecreulx, D., van Heijenoort, J., and Blanot, D. (1990) *Eur. J. Biochem 194*, 853−861.
12. Duncan, K., van Heijenoort, J., and Walsh, C. T. (1990) *Biochemistry 29*, 2379−2386.
13. Ikeda, M., Wachi, M., Jung, H. K., Ishino, F., and Matsuhashi, M. (1991) *J. Bacteriol. 173*, 1021−1026.
14. Mengin Lecreulx, D., Texier, L., Rousseau, M., and van Heijenoort, J. (1991) *J. Bacteriol. 173*, 4625−4636.
15. Bupp, K., and van Heijenoort, J. (1993) *J. Bacteriol. 175*, 1841−1843.
16. Maidhof, H., Reinicke, B., Blumel, P., Berger Bachi, B., and Labischinski, H. (1991) *J. Bacteriol. 173*, 3507−3513.
17. Ehlert, K., Schroder, W., and Labischinski, H. (1997) *J. Bacteriol. 179*, 7573−7576.
18. Kopp, U., Roos, M., Wecke, J., and Labischinski, H. (1996) *Microb. Drug. Resist. 2*, 29−41.
19. Wada, A., and Watanabe, H. (1998) *J. Bacteriol. 180*, 2759−2765.
20. Reynolds, P. E. (1988) In *Antibiotic Inhibition of Bacterial Cell Surface Assembly and Function* (Actor, P., Daneo-Moore, L., Higgins, M. L., Salton, M. R. J., and Shockman, G. D., Eds.) pp 343−351, American Society for Microbiology, Washington.
21. Wyke, A. W., Ward, J. B., Hayes, M. V., and Curtis, C. A. M. (1981) *Eur. J. Biochem. 119*, 389−393.
22. Skarzynski, T., Mistry, A., Wonacott, A., Hutchinson, S. E., Kelly, V. A., and Duncan, K. (1996) *Structure 4*, 1465−1474.
23. Benson, T. E., Filman, D. J., Walsh, C. T., and Hogle, J. M. (1995) *Nat. Struct. Biol. 2*, 644−653.
24. Bertrand, J. A., Auger, G., Fanchon, E., Martin, L., Blanot, D., van Heijenoort, J., and Dideberg, O. (1997) *EMBO J. 16*, 3416−3425.
25. Yan, Y., Munshi, S., Leiting, B., Anderson, M. S., Chrzas, J., and Chen, Z. (2000) *J. Mol. Biol. 304*, 435−345.
26. Ha, S., Walker, D., Shi, Y., and Walker, S. (2000) *Protein Sci. 9*, 1045−1052.
27. Michel, M., and Gutmann, L. (1997) *Lancet 349*, 1901−1906.
28. Van Duyne, G. D., Standaert, R. F., Karplus, P. A., Schreiber, S. L., and Clardy, J. (1993) *J. Mol. Biol. 229*, 105−124.
29. Collaborative Computational Project, No. 4. (1994) *Acta Crystallogr. D50*, 760−763.
30. Sheldrick, G. M., and Gould, R. O. (1995) *Acta Crystallogr. B51*, 423−431.
31. Otwinowski, Z. (1991) In *Isomorphous Replacement and Anomalous Scattering* (Wolf, W., Evans, P. R., and Leslie, A. G. W., Eds.) pp 80−86, SERC Daresbury Laboratory, Warrington.
32. Ramakrishnan, V., Finch, J. T., Graziano, V., Lee, P. L., and Sweet, R. M. (1993) *Nature 362*, 219−223.
33. Cowtan, K. D., and Main, P. (1993) *Acta Crystallogr. D49*, 148−157.
34. Cowtan, K. D., and Main, P. (1998) *Acta Crystallogr. D54*, 487−493.
35. Sack, J. S. (1988) *J. Mol. Graph. 6*, 224−225.
36. Brunger, A. T. (1996) *Methods Mol. Biol. 56*, 245−266.
37. Rice, L. M., and Brunger, A. T. (1994) *Proteins 19*, 277−290.
38. Brunger, A. T. (1988) *J. Mol. Biol. 203*, 803−16.
39. Jiang, J. S., and Brunger, A. T. (1994) *J. Mol. Biol. 243*, 100−115.
40. Brunger, A. T. (1992) *Nature 355*, 472−475.
41. Laskowski, R. A., MacAurthur, M. W., Moss, D. S., and Thorton, J. M. (1993) *J. Appl. Crystallogr. 26*, 283−291.
42. Kraulis, P. (1991) *J. Appl. Crystallogr. 24*, 946−950.
43. Merritt, E. A., and Bacon, D. J. (1997) *Methods Enzymol. 277*, 505−524.
44. Hendrickson, W. A. (1991) *Science 254*, 51−58.
45. Benson, T. E., Walsh, C. T., and Hogle, J. M. (1996) *Structure 4*, 47−54.
46. Murzin, A. G. (1996) *Cur. Op. Struct. Biol. 6*, 386-394.
47. Matthews, F. S., Chen, Z. W., Bellamy, H. D., and McIntire, W. S. (1991) *Biochemistry 30*, 238−247.
48. Mattevi, A., Fraaije, M. W., Mozzarelli, A., Olivi, L., Coda, A., and van Berkel, W. J. (1997) *Structure 5*, 907−20.
49. Dobbek, H., Gremer, L., Meyer, O., and Huber, R.(1999) *Proc. Natl. Acad. Sci. U.S.A. 96*, 8884−8889.
50. Rossman, M. G., Moras, D., and Olsen, K. W. (1974) *Nature 250*, 194−199.
51. Farmer, B. T., Constantine, K. L., Goldfarb, V., Friedrichs, M. S., Wittekind, M., Yanchunas, J., Robertson, J. G., and Mueller, L. (1996) *Nat. Struct. Biol. 3*, 995−997.
52. Constantine, K. L., Mueller, L., Goldfarb, V., Wittekind, M., Metzler, W. J., Yanchunas, J., Robertson, J. G., Malley, M. F., Friedrichs, M. S., and Farmer, B. T. (1997) *J. Mol. Biol. 267*, 1223−1246.
53. Dhalla, A. M., Yanchunas, J., Ho, H. T., Falk, P. J., Villafranca, J. J., and Robertson, J. G. (1995) *Biochemistry 34*, 5390−5402.
54. Benson, T. E., Walsh, C. T., and Massey, V. (1997) *Biochemistry 36*, 796−805.
55. Benson, T. E., Walsh, C. T., and Hogle, J. M. (1997) *Biochemistry 36*, 806−11.

BI002162D